Am J Nucl Med Mol Imaging 2024;14(1):13-21
www.ajnmmi.us /ISSN:2160-8407/ajnmmi0151795

Original Article

Molecular imaging reveals the heterogeneous progression of tumor cells and tumor stroma: a practice of FDG PET and FAPI PET in diagnosing PSMA-negative bone metastases of progressive prostate cancer

Lizhi Zhu[1*], Peng Chen[2*], Zhongqiu Guo[1], Fangdu Li[3], Xiu Luo[1], Xia Du[4], Liying Zhang[3], Changjing Zuo[1], Xiao Li[1]

[1]Department of Nuclear Medicine, Shanghai Changhai Hospital, Shanghai 200433, China; [2]Department of Nuclear Medicine, Shanghai Tenth People's Hospital, Tongji University School of Medicine, Shanghai 200072, China; [3]Department of Nuclear Medicine, Liqun Hospital, Putuo District, Shanghai 200333, China; [4]Department of Radiology, The Affiliated Hospital of Guizhou Medical University, Guiyang 550004, Guizhou, China. [*]Equal contributors.

Received June 16, 2023; Accepted November 15, 2023; Epub February 20, 2024; Published February 28, 2024

Abstract: Tumors are often with complex and heterogeneous biological processes, such as glycometabolism and fibrosis, which are the main biochemical pathways that determine therapeutic effects. Specifically, this study aims to assess the diagnosing performance of ^{18}F-FDG and ^{68}Ga-FAPI-04 PET for different stages of progressive bone metastases with PSMA-negative pathology. Bone metastatic mouse model of prostate cancer was constructed via intra-bone injection of PSMA-negative prostate cancer PC3 cells. Cellular uptakes of ^{18}F-FDG and ^{68}Ga-FAPI-04 were separately performed on PC3, NIH-3T3 (FAP-positive) and a mixture. ^{68}Ga-PSMA-11, ^{18}F-FDG and ^{68}Ga-FAPI-04 PET/CT imaging were performed at 2, 4 weeks after tumor cell transplantation. Furthermore, PSMA and FAP expression in bone metastases were assessed by immunohistochemistry, and then compared with the imageological findings. On the cellular level, the independent tracer uptake on the basis of glycometabolism and fibrosis was observed. For animal imaging, ^{68}Ga-PSMA-11 imaging showed weak or absent tracer uptake in PSMA-negative bone metastatic lesions. In contrast, ^{68}Ga-FAPI-04 PET of bone metastases had a higher uptake and tumor-to-muscle (T/M) ratio than ^{18}F-FDG PET that was relative steady during the observation, but T/M ratio of fibrosis gradually decreased with increasing tumor growth, which ranged from 5.11 ± 1.26 at 2 weeks to 3.54 ± 0.23 at 4 weeks, revealing the delayed formation of tumor stroma in rapid proliferation. In addition, PET imaging results were corroborated by immunohistochemical assessment. In conclusion, molecular imaging approach revealed the heterogeneous progression of tumor cells and tumor stroma of bone metastasis of prostate cancer, and further confirming the necessity of multi-molecular imaging in cancer imaging.

Keywords: Molecular imaging, heterogeneity, prostate cancer, prostate-specific membrane antigen, fibroblast activation protein, bone metastases, glycometabolism, fibrosis

Introduction

Prostate cancer (PCa) is the second most commonly diagnosed cancer worldwide and the fifth leading cause of cancer death in men worldwide [1]. The most common site of metastasis from prostate cancer is bone, occurring in 65%-80% of patients with advanced disease [2]. Bone metastases (BMs) in prostate cancer are associated with pathologic fractures, pain, and reduced survival [3]. PCa that has metastasized to the bone and visceral tissues is highly lethal with 5-year survival rates remaining at 30% [4]. The clinical course of PCa is highly heterogeneous, ranging from indolent to aggressive phenotypes [5]. Heterogeneity exists both among patients, with variable rates of progression, and within individual tumors, which can exhibit a mixture of molecular subtypes. For example, some patients show an indolent course with slow progression, while others rapidly develop lethal metastatic disease. PCa can contain mixtures of molecular subtypes, including TMPRSS2-ERG fusion, SPOP mutation, and others [6]. This heterogeneity, together with the overall prolonged natural history of PCa compared to other solid tumors, creates challenges in diagnosis, staging, and assessing treatment response [7]. Hence, precise diagnostic strategies are warranted to guide therapeutic decisions and improve management across the heterogeneous manifestations of PCa [8]. Molecular imaging approaches that capture different aspects of tumor phenotype may provide enhanced personalized information to meet this need [9].

Prostate-specific membrane antigen (PSMA) is commonly over-expressed in PCa [10], enabling for PSMA-targeted positron emission tomography (PSMA PET). Currently, recurrent PCa is the primary indication for PSMA PET, and the majority of published clinical data concentrated on this issue. In contrast to technetium-99m-methyl diphosphonate (^{99m}Tc-MDP) bone scan, PSMA PET is feasible to detect metastatic PCa earlier in patients who have undergone radical prostatectomy, modifying management in about half of the patients [11-13]. However, some patients have inter- or intra-lesional heterogeneity

at presentation, and some have tumor characteristics that are PSMA-negative, leading to false negative imaging findings [14]. Prior research indicated that PSMA PET results were negative when PSMA-negative tumor area was larger than 50% on immunohistochemistry (IHC), despite very high level of prostate-specific antigen (PSA) expression [15]. In addition, BMs could be PSMA-negative in up to 15% cases [16]. False-negative results in PSMA PET may mislead staging and assessment of therapeutic efficacy in PCa patients. Given this heterogeneity and risk of false negatives with single modality imaging, there is a need for personalized diagnostic strategies in PCa. Molecular imaging approaches that provide complementary biological information could help address this need. Multimodal imaging combining targets such as PSMA, glucose metabolism, and tumor microenvironment markers may improve characterization of heterogeneous PCa phenotypes.

Despite its widespread use, ^{18}F-FDG PET has limited utility for PCa imaging due to the typically low glucose metabolism of prostate tumors [17]. However, changes in glycometabolism during PCa progression, such as upregulation of GLUT transporters, provide a rationale for evaluating ^{18}F-FDG PET in advanced disease [18]. Furthermore, some studies have shown that ^{18}F-FDG PET can detect lesions in certain cases of PCa that are negative on ^{68}Ga-PSMA PET [19, 20]. The underlying mechanism for this discrepancy is unclear, but may involve neuroendocrine differentiation or other unknown factors inducing increased glycolysis. While ^{18}F-FDG is suboptimal for routine PCa imaging, these findings suggest it could serve as a complementary modality for patients with biochemical evidence of disease but negative ^{68}Ga-PSMA PET scans. Overall, ^{18}F-FDG PET may be a useful supplemental imaging tool in the subset of PCa patients with low or absent PSMA expression.

In addition to tumor cells, the prostate cancer microenvironment undergoes important changes during progression. Cancer-associated fibroblasts (CAFs) play an important role in the TME because they communicate with PCa cells, affecting their metabolism and vulnerability to medicines [21]. There is compelling evidence to support the role of CAFs in the tumorigenesis and progression of PCa. These roles are predominantly played via contact-dependent and paracrine-signaling processes that are shared by normal and activated fibroblasts that surround PCa cells [22]. A key marker of CAF activation is upregulation of fibroblast activation protein (FAP) expression. Imaging with FAP inhibitors may enable characterization of the tumor microenvironment. Recently, quinoline-based FAP inhibitors (FAPI) have demonstrated promising outcomes in the diagnosis of several cancer types including PCa, making them the hotspot of research in nuclear medicine and molecular imaging. Although the role of FAP in PCa has not yet been extensively evaluated, it appears as the potential to identify the lesion that is of negative or low PSMA expression [23].

Above all, glycometabolism and fibrosis were the two main progression in progressive development of tumor cells and tumor stroma. In the present study, bone metastasis mouse model of PCa bearing PSMA-negative prostate cancer cells was constructed as a typical model with heterogeneity. Three PET imaging methods (i.e., ^{18}F-FDG, ^{68}Ga-PSMA-11 and ^{68}Ga-FAPI-04) were performed in mouse models at different stages of tumor growth. The feasibility of FDG and FAPI PET as the diagnostic tool for the evaluation of progressive BMs with PSMA-negative prostate cancer was assessed.

Materials and methods

Preparation of ^{68}Ga-PSMA-11 and ^{68}Ga-FAPI-04 probe

The PSMA (HBED-CC-PSMA) and FAPI (DOTA-FAPI-04) precursor were purchased from Nice-Labeling Technology Co., Ltd. ^{68}Ga-PSMA-11 and ^{68}Ga-FAPI-04 were prepared in house. For ^{68}Ga-PSMA-11 preparation, the precursor PSMA-11 was dissolved in 1 mL 0.05 M NH_4OAc, and then mixed with 4 mL freshly eluted $^{68}GaCl_3$ (in 0.05 M HCl). The reaction system was heated to 100°C and maintained for 10 min. Radiochemical purity (RCP) was measured with a HPLC with radio-detector. An analysis column (Wondasil C18 Superb 5 μm 4.6 × 250 mm) was used with a flow rate of 1 mL/min, and parameters were set as solvent A: water/0.1% TFA, solvent B: acetonitrile/100%, gradient details: 0-13 min, 33%-67% B. For ^{68}Ga-FAPI-04 probe preparation, the same procedure as ^{68}Ga-PSMA-11 was performed.

^{18}F-FDG was purchased from Atom Kexing Pharmaceuticals, and quality control was performed with a TLC with radio-detector. 95% acetonitrile was used as the mobile phase, and silica gel thin layer chromatography plate was used as the stationary phase. The Rf of FDG was around 0.4-0.5.

Cell culture and cellular uptake

PSMA-negative PCa cell line PC3 and embryonic mouse fibroblast cell line NIH-3T3 were purchased from Cell Bank of Type Culture Collection of Chinese Academy of Sciences, Shanghai Institute of Cell Biology, Chinese Academy of Sciences. Cells were cultured in Dulbecco's Modified Eagle's Medium (DMEM, Gibco) or RPMI 1640 medium (RP1640, Gibco) supplemented with 10% fetal bovine serum (FBS, Gibco) at 37°C in 5% CO_2.

For cellular uptake of ^{68}Ga-PSMA-11, ^{18}F-FDG or ^{68}Ga-FAPI-04, 1 × 10^5 PC3 or NIH-3T3 in logarthmic growth phase were co-cultured with 0.37 MBq radiopharmaceuticals for one hour. Medium was removed, and cells were washed with PBS for three times. Cellular uptake was quantified with a gamma-counter.

For cellular uptake of ^{18}F-FDG or ^{68}Ga-FAPI-04 that was performed on cell mixture, PC3 and NIH-3T3 cells were mixed together in a 1:1 ratio and plated in 24-well plates at a total density of 1 × 10^5 cells/well. Cells were allowed to adhere overnight before radiotracer incubation. On experiment day, culture media was replaced with fresh

media containing 0.37 MBq of ^{18}F-FDG or ^{68}Ga-FAPI-04 and incubated for 1 hour at 37 °C. After incubation, media was removed and cells were gently washed 3 times with PBS. Cells were harvested and radioactivity was measured using a gamma-counter.

Bone metastasis model preparation

Male nude mice (8-10 weeks old, 18-20 g) were purchased from Vital River Laboratory Animal Technology Co., Ltd. Animals were housed under a 12-h light/12-h dark cycle and allowed free access to food and water. For mouse models, the leg of the anesthetized mouse was flexed. A 27-gauge syringe needle was inserted into the marrow cavity parallel to the long axis of the femur, followed by injection of 20 μL of PC3 cell suspension (1×10^6 cells per mouse). All mouse experiments were approved by and performed following the guidelines of the Institutional Animal Care and Use Committee at Changhai hospital.

^{18}F-FDG, ^{68}Ga-PSMA-11 and ^{68}Ga-FAPI-04 PET/CT scanning

^{18}F-FDG and ^{68}Ga-FAPI-04 PET/CT imaging was performed at 2, 4 weeks after tumor cell transplantation, respectively. ^{68}Ga-PSMA-11 PET/CT was performed at 4 weeks after tumor transplantation. ^{18}F-FDG, ^{68}Ga-PSMA-11 and ^{68}Ga-FAPI-04 PET/CT scans were carried out within two days, with at least 12 h between scans to allow for physical decay of the previous tracer before the next scan. Before PET measurements, mice were anesthetized by intraperitoneal injection of Lidocaine (3%, wt%). For ^{18}F-FDG PET/CT, mice were fasted for 6 h before injection of ^{18}F-FDG into the tail vein. The dosage of ^{18}F-FDG injection was 5.55-7.40 MBq. Data were acquired using a PET/CT scanner (Biograph64, Siemens, Germany) after 1 h of intravenous administration. Image acquisition parameters were set as follows: for CT, tube voltage is 120 kV; Tube current: 35 mA; Pitch: 1.0; Reconstruction layer thickness: 1 mm. PET data acquisition was obtained for 5 minutes per bed position. For ^{68}Ga-PSMA-11 and ^{68}Ga-FAPI-04 PET/CT scan, the injection dose and procedure were the same as above, except that the radiopharmaceutical were ^{68}Ga-PSMA-11 and ^{68}Ga-FAPI-04, respectively.

Image analysis

TureD system of post-processing workstation was used for corrected for attenuation and image reconstruction to form transverse plane, coronal plane and sagittal plane and generate 3D projection image. Regions of interest (ROIs) were manually outlined on the muscle, and bone metastases. The PET/CT workstation provides SUV (standardized uptake value) as the quantitative value. One experienced nuclear medicine physician was responsible for measuring the SUV_{max} value and calculating tumor-to-background ratios.

Hematoxylin & eosin staining and immunohistochemistry

All mice that underwent PET imaging were euthanized by cervical dislocation. The right hindlimb was dissected and fixed in 10% neutral-buffered formalin, and decalcified in formic acid. Paraffin-embedded sections were stained with hematoxylin & eosin (H&E) and immunohistochemistry (IHC) according to standard protocol. The expression of PSMA and anti-fibroblast activated protein α (FAPα) was quantified by using the IHC toolbox plugin in ImageJ software. The following primary antibodies were used: anti-PSMA mAb (1:250, ab133579, Abcam, Shanghai, China), anti-FAP mAb (1:100, ab53066, Abcam, Shanghai, China).

Quantification and statistical analysis

Data were presented as the mean ± standard deviation of at least n = 3. Comparisons were performed using an unpaired t test. A *P* value less than 0.05 was considered statistically significant. Data were analyzed using GraphPad Prism version 9.3 (GraphPad Prism Software).

Results

Synthesis and radiolabeling

As the clinical used radiopharmaceuticals, ^{18}F-FDG, ^{68}Ga-PSMA-11 and ^{68}Ga-FAPI-04 were automatically synthesized with a radiochemical purity of higher than 95%, guaranteeing the real represent of pathology-related tracer uptake. The typical radio-HPLC spectrum of ^{68}Ga-FAPI-04 and ^{68}Ga-PSMA-11 were as **Figure 1A**, **1B**, and the typical radio-TLC spectrum of ^{18}F-FDG was as **Figure 1C**.

Independent tracer uptake of ^{18}F-FDG and ^{68}Ga-FAPI-04

PC3 cells stand for the PSMA-negative model cell, and embryonic mouse fibroblast cell line NIH-3T3 stand for the FAP-positive model cell. The above two cells were independent with concomitant matrix in verifying PSMA- or FAP-related tracer uptake. All of the co-culture with radiopharmaceuticals were performed for one hour. ^{68}Ga-PSMA-11 uptake was minimal and equivalent in PC3 (0.25 ± 0.05%) and NIH-3T3 (0.29 ± 0.03%) cells, and no difference was observed (**Figure 2A**), confirming lack of PSMA expression.

^{18}F-FDG uptake was higher in PC3 cells (3.55 ± 0.37%) compared to NIH-3T3 cells (1.51 ± 0.57%), while ^{68}Ga-FAPI-04 uptake was lower in PC3 cells (0.91 ± 0.15%) versus NIH-3T3 cells (3.91 ± 0.35%) (**Figure 2B**). A FAP-negative biochemical nature of PC3 was proved. For mixed cultures containing equal numbers of PC3 and NIH-3T3 cells, ^{18}F-FDG and ^{68}Ga-FAPI-04 uptake levels were intermediate between the individual cell lines (**Figure 2C**). This supported the independence of glycolytic metabolism versus fibroblast targeting.

Image analysis

Figures 3 and **4** presents the typical PET/CT images, including ^{68}Ga-PSMA-11, ^{18}F-FDG and ^{68}Ga-FAPI-04 in a

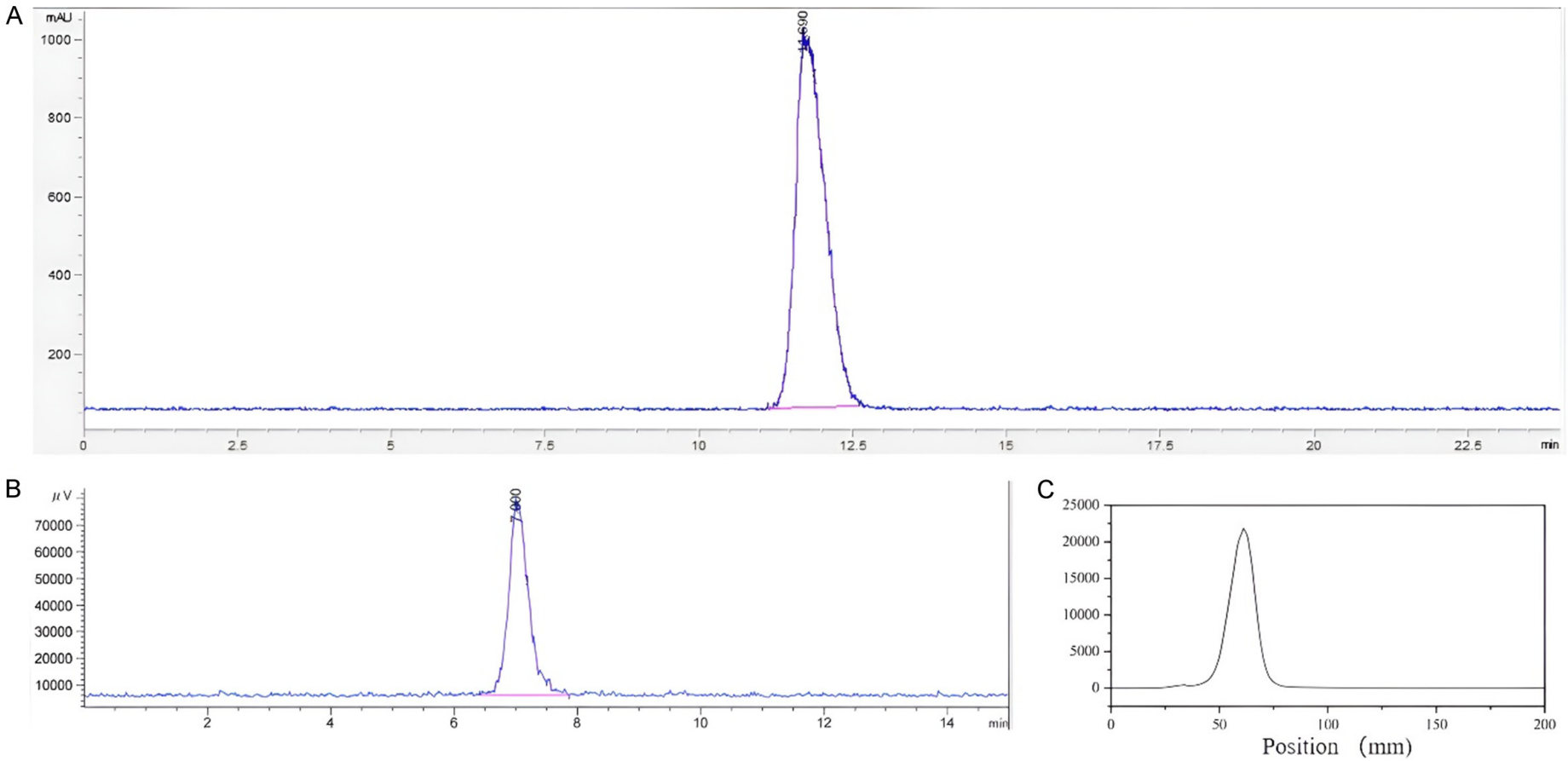

Figure 1. The typical radio-HPLC spectrum of ^{68}Ga-FAPI-04 (A) and ^{68}Ga-PSMA-11 (B), and the typical radio-TLC spectrum of ^{18}F-FDG (C).

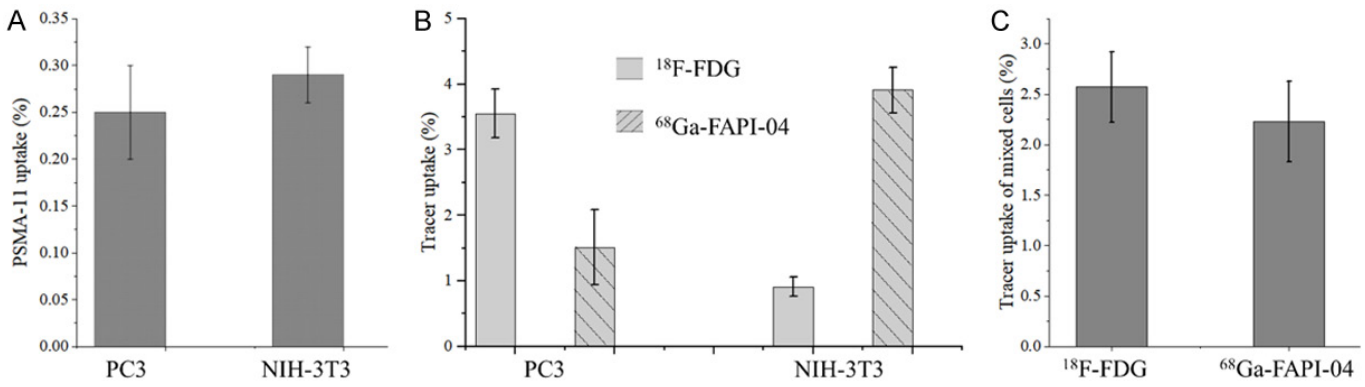

Figure 2. Cellular uptake of ^{68}Ga-PSMA-11, ^{18}F-FDG and ^{68}Ga-FAPI-04. A. Cellular uptake of ^{68}Ga-PSMA-11; B. Cellular uptake of ^{18}F-FDG and ^{68}Ga-FAPI-04; C. Cellular uptake of ^{18}F-FDG and ^{68}Ga-FAPI-04 in cell mixture.

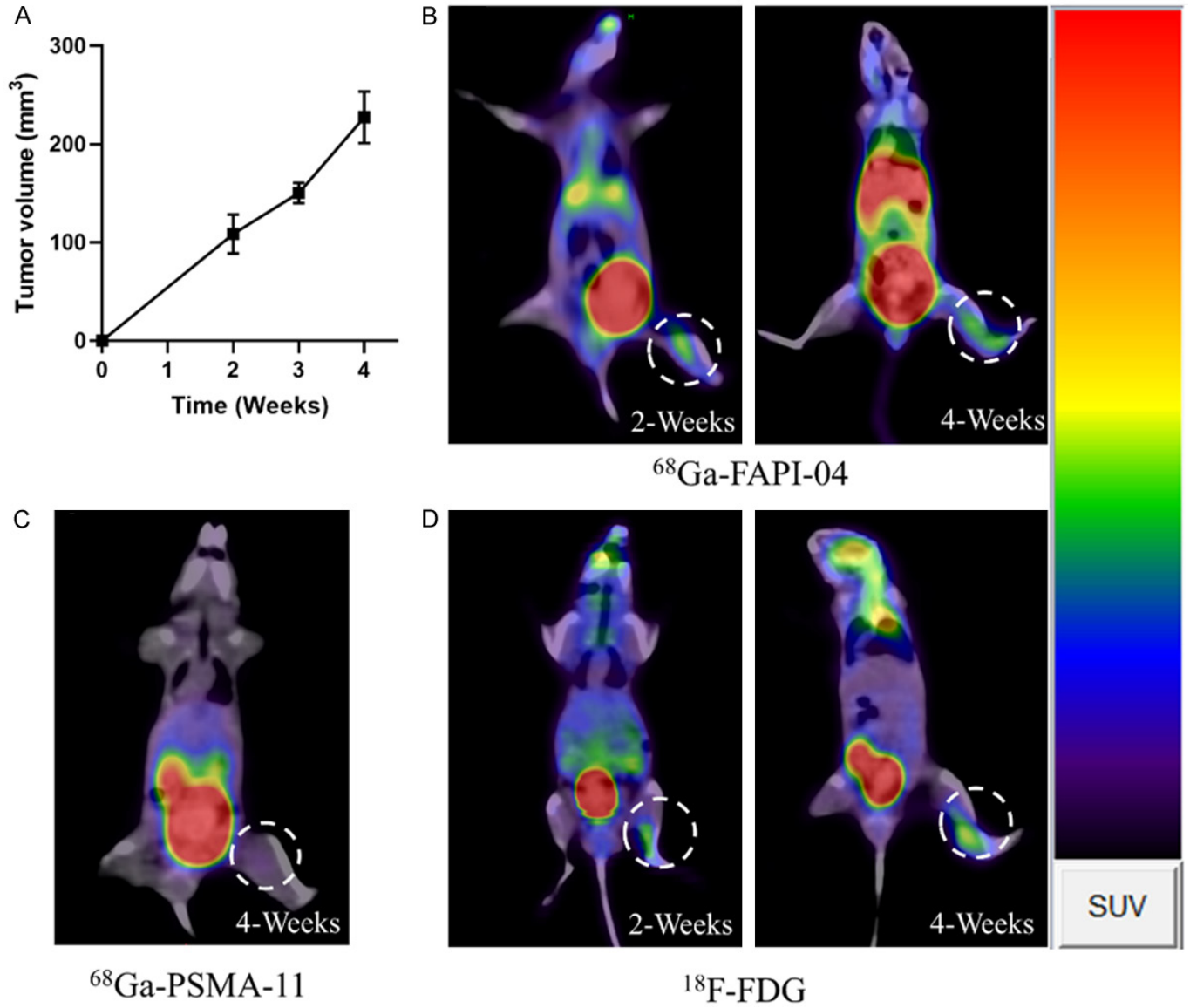

Figure 3. (A) Change in PC3 xenograft tumor volume after transplantation. The typical PET imaging of ^{68}Ga-FAPI-04 (B), ^{68}Ga-PSMA-11 (C) and ^{18}F-FDG (D) in mouse model bearing bone metastases with negative-PSMA expression at different time points after transplantation.

bone metastatic model, and corresponding quantitative data of mice at 2- and 4-week post tumor cell transplantation. As expected, ^{68}Ga-PSMA-11 imaging showed very weak or absent radiotracer uptake in BMs at 4 weeks

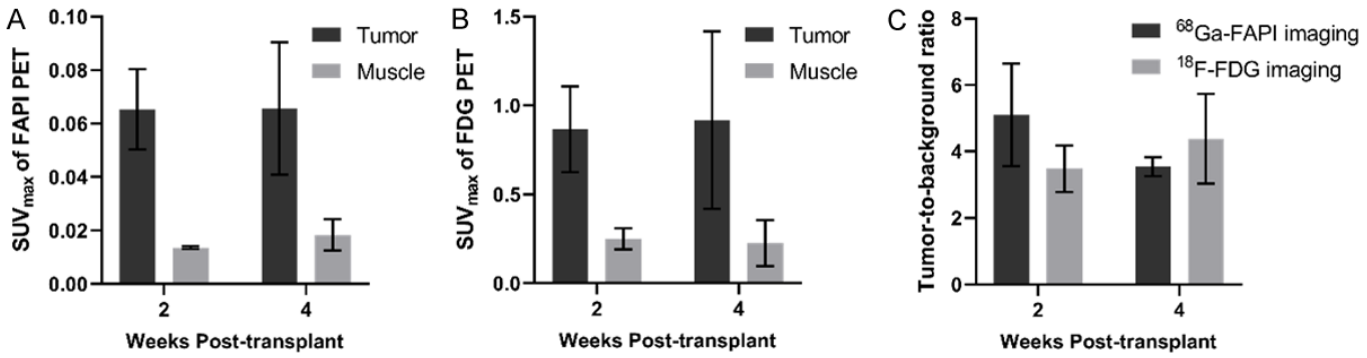

Figure 4. A. The SUV_{max} of ^{68}Ga-FAPI-04 in the bone metastases and muscle. B. The SUV_{max} of ^{18}F-FDG in the bone metastases and muscle. C. The tumor-to-background (muscle) ratio of ^{68}Ga-FAPI-04 and ^{18}F-FDG in the mouse at different time points after transplantation.

after transplantation. Weak uptake of tumor was due, in part, to nonspecific accumulation caused by increased tumor blood flow and vascular permeability. For the ^{18}F-FDG PET/CT images acquired at 60 min post injection, high radiotracer uptake was observed in the site of bone metastasis at 2 weeks after transplantation, with SUV_{max} of 0.87 ± 0.20. Two weeks later, ^{18}F-FDG PET/CT showed irregular mass shadow of high density, with increased radiotracer uptake in the site of bone metastasis, with SUVmax of 0.92 ± 0.41 (**Figure 4B**). The kidney and bladder displayed relatively high radioactivity accumulation at 60 min post injection. The radioactivity accumulation of the bladder was represented as the total excretion at 60 min post injection. Compared with FDG PET imaging at 2 weeks (T/M ratio was 3.48 ± 0.57), a high contrast of a T/M ratio of 4.38 ± 1.10 was achieved at 4 weeks post transplantation (**Figure 4C**).

For ^{68}Ga-FAPI-04 imaging, the BMs had a high uptake of ^{68}Ga-FAPI-04 at 2 and 4 weeks after transplantation (**Figure 4A**). Other organs demonstrated low nonspecific binding that quickly decreased, resulting in low background signal and favorable tumor-to-background ratios. T/M ratios gradually decreased with increasing tumor size, which ranged from 5.11 ± 1.26 at two weeks to 3.54 ± 0.23 at four weeks (**Figure 4C**).

In addition, the T/M ratio of ^{68}Ga-FAPI-04 was higher than that of ^{18}F-FDG (5.11 ± 1.26 vs. 3.48 ± 0.57, t = 1.657, P = 0.173) at 2 weeks post transplantation. The comparison of the T/M ratio of ^{68}Ga-FAPI-04 with that of ^{18}F-FDG was reversed at 4 weeks post tumor transplantation (3.54 ± 0.23 vs. 4.38 ± 1.10, t = 1.054, P = 0.351) (**Figure 4C**). In these cases, the high T/M ratio could clearly distinguish BMs from background visually, although there was no statistically significant difference between these two groups at both time points.

H&E and immunohistochemistry

In gross pathological anatomy, a mass was seen in the femur on the side of the PCa tumor cells inoculated, which was grayish-white and bulged outward. In histopathology of bone metastasis, a large number of epithelial cells in the bone marrow cavity and outside the bone cortex. The tumor cells were arranged in fascicles with obvious atypia, hyperchromatic with a large nucleus (**Figure 5A**, **5D**). IHC staining showed that the expression of PSMA was negative in bone metastasis tissues (**Figure 5B**, **5E**), while FAP was highly expressed, and the positive staining area of FAP was 21.51 ± 2.64% (**Figure 5C**, **5F**).

Above all, tumor progression was complicated and dynamic, hence, a single molecular imaging was miss-leading in understanding tumor status. The medical pictures of glycometabolism and fibrosis that were acquired at 2 and 4 weeks manifested the asynchronism of tumor progression and tumorous stroma formation.

Discussion

For individuals with PCa, early diagnosis of distant metastases is crucial for staging and therapeutic planning, but the diagnostic results relied on a sole imaging modality was somewhat unilateral in patient management. In the past few years, the use of ^{68}Ga-PSMA-11 PET/CT rapidly spread worldwide. Numerous studies have highlighted the high sensitivity of ^{68}Ga-PSMA-11 PET/CT in PCa patients as compared to other imaging modalities [24]. Of note, a few PCa types do not adequately express PSMA. However, there are limited studies of other imaging methods available for the detection of PCa patients that are of negative PSMA uptake [25, 26]. Therefore, despite patients' having high PSA levels, PSMA-based imaging may not indicate any pathological lesions [27].

^{18}F-FDG is frequently thought to perform poorly in PCa imaging because of its unique metabolic properties that result in a low affinity for glucose in metastatic lesions of PCa [28]. In our present study, ^{18}F-FDG PET/CT imaging could sensitively detect BMs lesions that were PSMA-negative in early-stage, and could continuously monitor the progressive changes of BMs. These results are consistent to the imaging findings of Chen et al. in patients with biochemical recurrent PCa [25], implying that ^{68}Ga-PSMA-11-negative patients with biochemical recurrence were likely to benefit from ^{18}F-FDG PET. Despite the potential for FDG imaging in PSMA-negative tumors, the reason

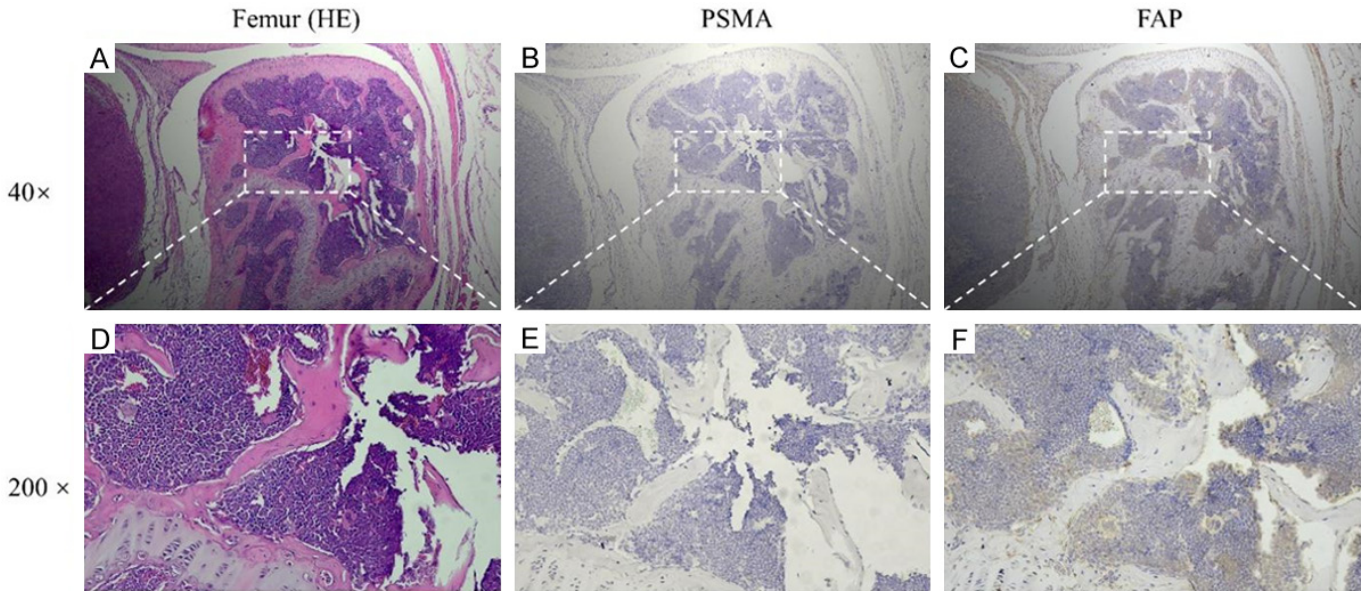

Figure 5. Hematoxylin & eosin and immunohistochemical staining of FAP and PSMA expression in bone metastatic lesion of PCa. A, D. Photomicrograph of H&E-stained bone metastatic lesion (40 × and 200 ×, respectively); B, E. Bone metastatic lesion demonstrated negative PSMA expression on immunohistochemistry (40 × and 200 ×, respectively); C, F. Fibroblast activation protein-α (FAP-α) staining in bone metastatic tissues, showing high expression of FAP-α in tumor stroma (40 × and 200 ×, respectively).

behind these imaging findings is unclear. One reason may be involved in other yet-unknown physiological or pathological conditions, such as neuroendocrine differentiation in prostate cancer. Bakht et al. revealed that high levels of glucose uptake were correlated to a suppression of PSMA and an elevation of neuroendocrine biomarkers [29]. Conversely, several reports showed that neuroendocrine differentiation of PCa was not associated with increased ^{18}F-FDG uptake [30]. Albeit plausible, this mechanism awaits further research and validation. However, we still recommend FDG PET as an essential tool for PSMA-negative imaging, especially for progressive PCa diagnosis and treatment monitoring.

Although the molecular markers of tumor cells are significantly different and even deficient, the tumor microenvironment has similar characteristics. CAFs are a pivotal component of stroma, accounting for 90% of the total tumor mass in desmoplastic tumors. The PCa-promoting characteristics of CAFs have been shown in numerous research, including raising tumorigenic potential, improving androgen sensitivity, and favoring the metastatic process [31-33]. Because CAFs are genetically more stable than cancer cells, diagnostic and therapeutic targeting of CAFs in the stroma has distinct advantages and potential. In this study, we hypothesized that FAP imaging could serve as a potential diagnostic tracer targeting CAFs for PSMA-negative PCa, and a robust uptake of the FAPI tracer was observed in the PSMA-negative BMs. The imaging results were corroborated by immunohistochemical studies using FAPα antibody. Additionally, high tumor-to-background contrast was paramount for tumor imaging. In the present study, a relative high T/M ratio in FAPI imaging, up to 5.11 ± 1.26 were observed. Furthermore, we also found that T/M ratio of ^{68}Ga-FAPI-04 imaging was higher than that of ^{18}F-FDG imaging in the early-stage of BMs development, implying that stroma formation accompanied with BMs and was more active in early stage, but the delayed formation of tumor stroma in rapid proliferation was observed as well. Hence, the additive value of FAPI imaging was exhibited by the enhanced T/M ratios, increasing the confidence in the lesion diagnosis.

Nevertheless, little is known regarding FAP expression in various disease stages of PCa. According to a recent study by Hintz et al., FAP expression is a characteristic of metastatic castration-resistant PCa regardless of genetic subtype, therapeutic strategy, or metastatic site. Moreover, they found that a significant increase in FAP mRNA expression in metastatic disease compared to primary PCa [34]. Similarly, in a separate clinical trial, Kesch et al. indicated that ^{68}Ga-FAPI-04 PET/CT was highly positive in subjects with advanced castration-resistant PCa [35]. These data were consistent with our results and further provided a rationale for FAPI imaging as a potential diagnostic tool for PCa, particularly in patients with heterogeneous tumor phenotypes. Notably, the nature of FAP expression is very non-specific in a mixed illness environment and at early diagnosis because it is related to chronic inflammation, including but not limited to, rheumatoid arthritis, fibroses, and wound healing. Hence, we stressed that due to its lack of specificity, single-step imaging with FAP may not be helpful for the early identification of PCa. Patients with PSMA-negative or PSMA-expression heterogeneity may benefit more from FAP imaging for PCa diagnosis, as well as the potential of FAPI-targeted theranostic in PCa. Large-scale randomized clinical trials are further required to generate definitive evidence.

FDG PET is known to have limited specificity for cancer due to uptake in sites of inflammation and infection. Similarly, FAP expression occurs in wound healing, fibrosis and other conditions, reducing specificity of FAPI PET when interpreted alone. Caution is warranted when evaluating either scan, or correlation with clinical context is key for accurate interpretation. For PCa, FDG and FAPI PET may be the most suitable for assessing advanced disease where PSMA imaging falls short. FDG could identify morphological and metabolic alterations associated with aggressive tumors [36]. FAPI may detect stromal remodeling during progression to castration resistance [35]. However, questions remain regarding appropriate clinical use cases, influence of therapies, and ability to improve patient outcomes. Larger prospective studies are needed to define applications and limitations.

In summary, while FDG and FAPI PET hold promise for characterizing prostate cancer in certain scenarios, care is required when applying these modalities clinically due to non-specificity issues. Additional research is needed to realize their full potential while mitigating limitations.

This study has several potential limitations. Firstly, the experimental model was the transplantation of PSMA-negative PCa cells into the femur of mice, which were poorly able to sufficiently mimic the bone metastatic progression after the occurrence of orthotopic prostate tumor formation, as in the human disease. Secondly, FDG and FAPI imaging for different pathological subtypes and different course of prostate cancer were not evaluated due to objective limitations of the mouse model.

Conclusions

This study revealed the feasibility of ^{18}F-FDG and ^{68}Ga-FAPI-04 PET/CT as the complementary diagnostic tool for bone metastasis of PCa with negative PSMA-expression. Due the complexity of tumor progression, FDG and FAP-targeted imaging may be valuable as a candidate application for the PCa patients with PSMA-negative or PSMA-expression heterogeneity, especially for tumor cell proliferation and tumor stroma.

Acknowledgements

This research was supported by the National Natural Science Foundation of China (81871390, 82272040), and the First Affiliated Hospital of Naval Medical University (Shanghai Changhai Hospital) “Guhai Plan in the 14th Five-Year Plan period” (GH145-22).

Disclosure of conflict of interest

None.

Address correspondence to: Xia Du, Department of Radiology, The Affiliated Hospital of Guizhou Medical University, Guiyang 550004, Guizhou, China. E-mail: duxia05@126.com; Liying Zhang, Department of Nuclear Medicine, Liqun Hospital, Putuo District, Shanghai 200333, China. E-mail: verazh771125@qq.com

References

[1] Sung H, Ferlay J, Siegel RL, Laversanne M, Soerjomataram I, Jemal A and Bray F. Global cancer statistics 2020: GLOBOCAN estimates of incidence and mortality worldwide for 36 cancers in 185 countries. CA Cancer J Clin 2021; 71: 209-249.

[2] Weilbaecher KN, Guise TA and McCauley LK. Cancer to bone: a fatal attraction. Nat Rev Cancer 2011; 11: 411-425.

[3] Armstrong AJ, Anand A, Edenbrandt L, Bondesson E, Bjartell A, Widmark A, Sternberg CN, Pili R, Tuvesson H, Nordle Ö, Carducci MA and Morris MJ. Phase 3 assessment of the automated bone scan index as a prognostic imaging biomarker of overall survival in men with metastatic castration-resistant prostate cancer: a secondary analysis of a randomized clinical trial. JAMA Oncol 2018; 4: 944-951.

[4] Leibold J, Ruscetti M, Cao Z, Ho YJ, Baslan T, Zou M, Abida W, Feucht J, Han T, Barriga FM, Tsanov KM, Zamechek L, Kulick A, Amor C, Tian S, Rybczyk K, Salgado NR, Sánchez-Rivera FJ, Watson PA, de Stanchina E, Wilkinson JE, Dow LE, Abate-Shen C, Sawyers CL and Lowe SW. Somatic tissue engineering in mouse models reveals an actionable role for WNT pathway alterations in prostate cancer metastasis. Cancer Discov 2020; 10: 1038-1057.

[5] Parker C, Castro E, Fizazi K, Heidenreich A, Ost P, Procopio G, Tombal B and Gillessen S; ESMO Guidelines Committee. Electronic address: clinicalguidelines@esmo.org. Prostate cancer: ESMO clinical practice guidelines for diagnosis, treatment and follow-up. Ann Oncol 2020; 31: 1119-1134.

[6] Fontana F, Anselmi M and Limonta P. Molecular mechanisms and genetic alterations in prostate cancer: from diagnosis to targeted therapy. Cancer Lett 2022; 534: 215619.

[7] Gandaglia G, Leni R, Bray F, Fleshner N, Freedland SJ, Kibel A, Stattin P, Van Poppel H and La Vecchia C. Epidemiology and prevention of prostate cancer. Eur Urol Oncol 2021; 4: 877-892.

[8] Alipour R, Azad A and Hofman MS. Guiding management of therapy in prostate cancer: time to switch from conventional imaging to PSMA PET? Ther Adv Med Oncol 2019; 11: 1758835919876828.

[9] Jetty S, Loftus JR, Patel A, Gupta A, Puri S and Dogra V. Prostate cancer-PET imaging update. Cancers (Basel) 2023; 15: 796.

[10] Hofman MS, Hicks RJ, Maurer T and Eiber M. Prostate-specific membrane antigen PET: clinical utility in prostate cancer, normal patterns, pearls, and pitfalls. Radiographics 2018; 38: 200-217.

[11] Pyka T, Okamoto S, Dahlbender M, Tauber R, Retz M, Heck M, Tamaki N, Schwaiger M, Maurer T and Eiber M. Comparison of bone scintigraphy and 68Ga-PSMA PET for skeletal staging in prostate cancer. Eur J Nucl Med Mol Imaging 2016; 43: 2114-2121.

[12] Mena E, Lindenberg ML, Shih JH, Adler S, Harmon S, Bergvall E, Citrin D, Dahut W, Ton AT, McKinney Y, Weaver J, Eclarinal P, Forest A, Afari G, Bhattacharyya S, Mease RC, Merino MJ, Pinto P, Wood BJ, Jacobs P, Pomper MG, Choyke PL and Turkbey B. Clinical impact of PSMA-based

18F-DCFBC PET/CT imaging in patients with biochemically recurrent prostate cancer after primary local therapy. Eur J Nucl Med Mol Imaging 2018; 45: 4-11.
[13] Han S, Woo S, Kim YJ and Suh CH. Impact of 68Ga-PSMA PET on the management of patients with prostate cancer: a systematic review and meta-analysis. Eur Urol 2018; 74: 179-190.
[14] Paschalis A, Sheehan B, Riisnaes R, Rodrigues DN, Gurel B, Bertan C, Ferreira A, Lambros MBK, Seed G, Yuan W, Dolling D, Welti JC, Neeb A, Sumanasuriya S, Rescigno P, Bianchini D, Tunariu N, Carreira S, Sharp A, Oyen W and de Bono JS. Prostate-specific membrane antigen heterogeneity and DNA repair defects in prostate cancer. Eur Urol 2019; 76: 469-478.
[15] Ferraro DA, Rüschoff JH, Muehlematter UJ, Kranzbühler B, Müller J, Messerli M, Husmann L, Hermanns T, Eberli D, Rupp NJ and Burger IA. Immunohistochemical PSMA expression patterns of primary prostate cancer tissue are associated with the detection rate of biochemical recurrence with 68Ga-PSMA-11-PET. Theranostics 2020; 10: 6082-6094.
[16] Mannweiler S, Amersdorfer P, Trajanoski S, Terrett JA, King D and Mehes G. Heterogeneity of prostate-specific membrane antigen (PSMA) expression in prostate carcinoma with distant metastasis. Pathol Oncol Res 2009; 15: 167-172.
[17] Jadvar H. Imaging evaluation of prostate cancer with 18F-fluorodeoxyglucose PET/CT: utility and limitations. Eur J Nucl Med Mol Imaging 2013; 40 Suppl 1: S5-10.
[18] Gonzalez-Menendez P, Hevia D, Mayo JC and Sainz RM. The dark side of glucose transporters in prostate cancer: are they a new feature to characterize carcinomas? Int J Cancer 2018; 142: 2414-2424.
[19] Parida GK, Tripathy S, Datta Gupta S, Singhal A, Kumar R, Bal C and Shamim SA. Adenocarcinoma prostate with neuroendocrine differentiation: potential utility of 18F-FDG PET/CT and 68Ga-DOTANOC PET/CT Over 68Ga-PSMA PET/CT. Clin Nucl Med 2018; 43: 248-249.
[20] Perez PM, Hope TA, Behr SC, van Zante A, Small EJ and Flavell RR. Intertumoral heterogeneity of 18F-FDG and 68Ga-PSMA uptake in prostate cancer pulmonary metastases. Clin Nucl Med 2019; 44: e28-e32.
[21] Bedeschi M, Marino N, Cavassi E, Piccinini F and Tesei A. Cancer-associated fibroblast: role in prostate cancer progression to metastatic disease and therapeutic resistance. Cells 2023; 12: 802.
[22] Bonollo F, Thalmann GN, Kruithof-de Julio M and Karkampouna S. The role of cancer-associated fibroblasts in prostate cancer tumorigenesis. Cancers (Basel) 2020; 12: 1887.
[23] Khreish F, Rosar F, Kratochwil C, Giesel FL, Haberkorn U and Ezziddin S. Positive FAPI-PET/CT in a metastatic castration-resistant prostate cancer patient with PSMA-negative/FDG-positive disease. Eur J Nucl Med Mol Imaging 2020; 47: 2040-2041.
[24] Esen T, Kılıç M, Seymen H, Acar Ö and Demirkol MO. Can Ga-68 PSMA PET/CT replace conventional imaging modalities for primary lymph node and bone staging of prostate cancer?. Eur Urol Focus 2020; 6: 218-220.
[25] Chen R, Wang Y, Shi Y, Zhu Y, Xu L, Huang G and Liu J. Diagnostic value of 18F-FDG PET/CT in patients with biochemical recurrent prostate cancer and negative 68Ga-PSMA PET/CT. Eur J Nucl Med Mol Imaging 2021; 48: 2970-2977.
[26] Pang Y, Meng T, Xu W, Shang Q and Chen H. 68 Ga-FAPI PET/CT detected non-PSMA/FDG-avid primary tumor in de novo metastatic prostate cancer. Clin Nucl Med 2022; 47: 1108-1111.
[27] Afshar-Oromieh A, Babich JW, Kratochwil C, Giesel FL, Eisenhut M, Kopka K and Haberkorn U. The rise of PSMA ligands for diagnosis and therapy of prostate cancer. J Nucl Med 2016; 57 Suppl 3: 79S-89S.
[28] Zhu A, Lee D and Shim H. Metabolic positron emission tomography imaging in cancer detection and therapy response. Semin Oncol 2011; 38: 55-69.
[29] Bakht MK, Lovnicki JM, Tubman J, Stringer KF, Chiaramonte J, Reynolds MR, Derecichei I, Ferraiuolo RM, Fifield BA, Lubanska D, Oh SW, Cheon GJ, Kwak C, Jeong CW, Kang KW, Trant JF, Morrissey C, Coleman IM, Wang Y, Ahmadzadehfar H, Dong X and Porter LA. Differential expression of glucose transporters and hexokinases in prostate cancer with a neuroendocrine gene signature: a mechanistic perspective for 18F-FDG imaging of PSMA-suppressed tumors. J Nucl Med 2020; 61: 904-910.
[30] Bauckneht M, Morbelli S, Miceli A, Rebuzzi SE and Fornarini G. Neuroendocrine differentiation of prostate cancer is not systematically associated with increased 18F-FDG uptake. Diagnostics (Basel) 2021; 11: 468.
[31] Thalmann GN, Rhee H, Sikes RA, Pathak S, Multani A, Zhau HE, Marshall FF and Chung LW. Human prostate fibroblasts induce growth and confer castration resistance and metastatic potential in LNCaP cells. Eur Urol 2010; 58: 162-171.
[32] Wen S, Niu Y, Yeh S and Chang C. BM-MSCs promote prostate cancer progression via the conversion of normal fibroblasts to cancer-associated fibroblasts. Int J Oncol 2015; 47: 719-727.
[33] Sun DY, Wu JQ, He ZH, He MF and Sun HB. Cancer-associated fibroblast regulate proliferation and migration of prostate cancer cells through TGF-β signaling pathway. Life Sci 2019; 235: 116791.
[34] Hintz HM, Gallant JP, Vander Griend DJ, Coleman IM, Nelson PS and LeBeau AM. Imaging fibroblast activation protein alpha improves diagnosis of metastatic prostate cancer with positron emission tomography. Clin Cancer Res 2020; 26: 4882-4891.
[35] Kesch C, Yirga L, Dendl K, Handke A, Darr C, Krafft U, Radtke JP, Tschirdewahn S, Szarvas T, Fazli L, Gleave M, Giesel FL, Haberkorn U and Hadaschik B. High fibroblast-activation-protein expression in castration-resistant prostate cancer supports the use of FAPI-molecular theranostics. Eur J Nucl Med Mol Imaging 2021; 49: 385-389.
[36] Kostakoglu L, Agress H Jr and Goldsmith SJ. Clinical role of FDG PET in evaluation of cancer patients. Radiographics 2003; 23: 315-340; quiz 533.